Title
Processing of microRNA primary transcripts requires heme in mammalian cells

Journal
Proceedings of the National Academy of Sciences of the United States of America, 111(5)

ISSN
0027-8424

Authors
Weitz, Sara H
Gong, Ming
Barr, Ian
et al.

Publication Date
2014-02-04

DOI
10.1073/pnas.1309915111

Peer reviewed

Processing of microRNA primary transcripts requires heme in mammalian cells

Sara H. Weitz[a], Ming Gong[b], Ian Barr[b], Shimon Weiss[c,d,1], and Feng Guo[b,1]

[a]Interdepartmental Program in Molecular, Cellular, and Integrative Physiology, [b]Department of Biological Chemistry, David Geffen School of Medicine, [c]Department of Chemistry and Biochemistry, and [d]Department of Physiology, David Geffen School of Medicine, University of California, Los Angeles, CA 90095

Edited by David P. Bartel, Massachusetts Institute of Technology, Cambridge, MA, and approved December 24, 2013 (received for review May 29, 2013)

DiGeorge syndrome critical region gene 8 (DGCR8) is the RNA-binding partner protein of the nuclease Drosha. DGCR8 and Drosha recognize and cleave primary transcripts of microRNAs (pri-miRNAs) in the maturation of canonical microRNAs (miRNAs) in animals. We previously reported that human, frog, and starfish DGCR8 bind heme when expressed in *Escherichia coli* and that Fe (III) heme activates apoDGCR8 in reconstituted pri-miRNA processing assays. However, the physiological relevance of heme in miRNA maturation has not been clear. Here, we present a live-cell pri-miRNA processing assay that produces robust signals and faithfully indicates DGCR8 and Drosha activities. We demonstrate that all known heme-binding–deficient DGCR8 mutants are defective in pri-miRNA processing in HeLa cells. DGCR8 contains a previously uncharacterized heme-binding motif, "IPCL," that is also required for its activity. Heme availability and biosynthesis in HeLa cells positively affect pri-miRNA processing and production of mature miRNA. These results establish an essential function for heme in pri-miRNA processing in mammalian cells. Our study suggests that abnormal heme biosynthesis and degradation may contribute to diseases via miRNA-mediated gene regulation networks.

iron | protoporphyrin IX | RNA processing | noncoding RNA | fluorescence microscopy

MicroRNAs (miRNAs) are small noncoding RNAs (~20–22 nt) that regulate gene expression via specific targeting of mRNAs for degradation and translation inhibition (1–3). A miRNA is initially produced as a long primary transcript (pri-miRNA), which is processed by the Microprocessor, a complex composed of the ribonuclease Drosha and an RNA-binding protein DiGeorge syndrome critical region gene 8 (DGCR8) (or Pasha, the fly and worm homologs of DGCR8) (4–11). The resulting precursor miRNA (pre-miRNA) is exported into the cytoplasm by Exportin-5 where it is processed further by Dicer and subsequently loaded into RISC (RNA-induced silencing complex) (12, 13). Abundant evidence indicates that pri-miRNA processing is highly regulated during development and is often dysregulated in diseases (1, 14, 15). For example, p53, lin-28B, and SMAD proteins have been shown to directly regulate the Microprocessor complex (16–18). In addition, DiGeorge syndrome is caused by the chromosomal deletion 22q11.2, a section that includes DGCR8 (19). A mouse model for this deletion shows that haploinsufficiency of *Dgcr8* results in abnormal miRNA biogenesis in the brain that contributes to the neurological and behavioral defects associated with DiGeorge syndrome (20, 21).

Studying pri-miRNA processing in cells has been technically challenging. Mature miRNAs are generally believed to be long-lived molecules although accelerated decay for individual microRNAs has been reported (22). Thus, the abundance of miRNAs often does not change dramatically unless cells grow by proliferation or differentiation. Furthermore, the Drosha-cleavage step is coupled to cell growth in certain cell types (23). Finally, unprocessed pri-miRNAs seem to be degraded quickly via a pathway not well understood, and thus do not greatly accumulate. Two cellular reporter assays for pri-miRNA processing have been previously described. A fluorescence-based assay comprises a GFP–pri-miRNA fusion construct that is stably integrated into various cell lines (24). This assay suffers from the lack of a normalization factor to overcome variability in fluorescent protein expression due to processes unrelated to pri-miRNA processing. The second system uses a firefly luciferase–pri-miRNA fusion and normalizes the firefly luciferase signal to that of Renilla luciferase expressed from a cotransfected plasmid (25). However, as the luciferase expression levels are measured enzymatically in cell lysates, single-cell resolution and real-time experiments cannot be achieved.

An outstanding question about miRNA maturation concerns a potential role for heme in pri-miRNA processing. We previously found that a truncated form of the 773-residue DGCR8 called NC1 (amino acids 276–751) overexpressed in *Escherichia coli* stably associates with heme (26). Each DGCR8 dimer associates with one heme molecule using a heme-binding domain (HBD) located in its central region (amino acids 276–498) and ligates to the heme iron using the Cys352 residues from both subunits (27, 28). Through mutagenesis analyses, Cys352 and Trp329 have been identified to be important for association with heme (27). We also identified the N-terminal region of the HBD as a dimerization domain (amino acids 276–353) and determined the crystal structures of this domain from human and frog DGCR8 (27). The structures show that DGCR8 makes an unconventional use of its WW motif for mediating an extensive dimerization interface. Interestingly, Cys352 and Trp329 from both subunits cluster on a common surface, which is likely to serve as a direct binding site for heme. The heme-free C352A, W329A, and W329H NC1 mutants display reduced but still substantial pri-miRNA processing activity in vitro (26, 27). It is

Significance

MicroRNAs (miRNAs) have important functions in development and cell physiology. The vast majority of mature miRNAs are produced from primary transcripts of microRNAs (pri-miRNAs) by a multi-step pathway. The first step, cleavage of pri-miRNAs by the Microprocessor complex, is highly regulated but technically challenging to study. We have developed a robust method that faithfully measures pri-miRNA processing efficiency in live cells. Using this assay, we establish an essential function of heme in miRNA maturation, a provocative idea suggested by previous biochemical studies. Our study reveals a previously unknown cellular function of this central biological cofactor, linking metal ion biology with the regulation of noncoding RNAs. Our method should be widely useful for studying RNA processing in biology and diseases.

Author contributions: S.H.W., S.W., and F.G. designed research; S.H.W., M.G., and I.B. performed research; S.H.W. and I.B. analyzed data; and S.H.W. and F.G. wrote the paper.

The authors declare no conflict of interest.

This article is a PNAS Direct Submission.

[1]To whom correspondence may be addressed. E-mail: sweiss@chem.ucla.edu or fguo@mbi.ucla.edu.

This article contains supporting information online at www.pnas.org/lookup/suppl/doi:10.1073/pnas.1309915111/-/DCSupplemental.

not clear that, in compartmentalized eukaryotic cells where heme is synthesized in the mitochondrion and DGCR8 functions in the nucleus, heme can really affect pri-miRNA processing.

Here, we report a live-cell pri-miRNA processing assay using a ratiometric fluorescence reporter that allows robust data analyses at single-cell resolution. Using this assay in combination with results from heme-binding analyses, we provide clear evidence that heme is essential for pri-miRNA processing in human cells.

Results

A Fluorescence-Based Live-Cell Pri-miRNA Processing Reporter. We designed a ratiometric reporter construct based on a plasmid that simultaneously expresses two fluorescent proteins, mCherry and eYFP, driven by a bidirectional tetracycline-inducible promoter (Fig. 1*A*). This plasmid was generated by Sharp, Mukherji, and co-workers for examining interactions between mature miRNAs and 3′-untranslated regions (UTRs) of target messenger RNAs (29). In our reporter, pri-miRNA sequences were inserted into the 3′-UTR of the mCherry expression cassette whereas the eYFP 3′-UTR was left unaltered. Thus, this construct expresses an mCherry–pri-miRNA fusion RNA. Cleavage of the pri-miRNA moiety of the fusion RNA by Drosha/DGCR8 results in removal of the polyadenylation (poly-A) tail along with a portion of the 3′-UTR, which leads to degradation of the mCherry mRNA and reduction of mCherry protein expression and its fluorescent signal. The eYFP fluorescence signal allows changes of individual cells' transcriptional and translational activities to be normalized. Thus, the mCherry/eYFP ratio should negatively correlate with pri-miRNA processing activity. In this study, we chose to use the reciprocal, the eYFP/mCherry ratio, as it is a positive indicator for pri-miRNA processing efficiency.

As a starting point, we engineered human pri-miR-9-1 and pri-miR-30a into our fluorescent reporter. HeLa cells transiently transfected with either the pri-miR-9-1 or pri-miR-30a fluorescent reporter showed expression of eYFP and mCherry (Fig. 1*B*). Not surprisingly, there was a large intrinsic variation in the expression levels of eYFP and mCherry among cells. The eYFP and mCherry intensities of individual cells had a linear relationship over the range of reporter expression levels achieved, indicating that the reporters make proportional responses to the pri-miRNA processing machinery (Fig. 1*C*). No plateauing was observed, suggesting that the reporter system had not saturated the endogenous processing machinery. We calculated the slope from linear regression of the data to measure the overall efficiency of pri-miRNA processing.

We validated the fluorescent reporters by ectopically expressing DGCR8. HeLa cells express DGCR8 at a relatively low level (30); thus, we expected that expression of functional DGCR8 protein from a plasmid would increase the efficiency of pri-miRNA processing. Cells were cotransfected with a reporter and a plasmid expressing an N-terminal flag-tagged DGCR8 protein (N-flag-DGCR8) (Fig. 1*D*). The C-terminal tail of DGCR8 has been shown to be required for pri-miRNA processing (31, 32), and a mutant with the C-terminal tail deleted (ΔCTT) was used as an inactive control (Fig. 1*D*). When N-flag-DGCR8 was ectopically expressed, we continually observed a 90% increase in the slope (Fig. 1*E* and Fig. S1 *A*, *B*, *D*, and *E*). In contrast, no significant changes in slope were observed in cells expressing the ΔCTT mutant.

We next tested whether the fluorescent signals faithfully indicate the processing of pri-miRNAs in cells. We used quantitative RT-PCR (qRT-PCR) to determine the abundance of the mCherry–pri-miRNA fusion RNAs, the eYFP mRNA and mature miRNA. Consistent with the fluorescence measurements, the eYFP/mCherry–pri-miRNA RNA expression ratio increased by about twofold in cells expressing N-flag-DGCR8 (Fig. 1*F* and Fig. S1*F*). The levels of mature miR-9 and miR-30a in cells ectopically expressing N-flag-DGCR8 increased to 1.7- and 1.6-fold of those in cells transfected with reporters only (Fig. 1*G* and Fig. S1*G*). HeLa cells do not naturally express miR-9 so the reporter solely contributes the signal, whereas the mature miR-30a detected here originates from both the highly expressed endogenous gene and the reporter. We confirmed the mature miR-9 qRT-PCR results using Northern blots (Fig. S1*C*). Additionally, we observed an increase in the pre-miR-9 after N-flag-DGCR8 expression, which is consistent with an increase in pri-miR-9-1 processing (Fig. S1*C*). In contrast to the wild-type N-flag-DGCR8, expression of ΔCTT did not cause large changes to the abundance of mCherry–pri-miRNA fusion, mature miR-9, or miR-30a relative to the "reporter only" transfection. Additionally, we tested a pri-miR-9-1 reporter in which the Drosha cleavage site was mutated, and this reporter was unresponsive to N-flag-DGCR8 expression (*SI Text* and Fig. S2). These results clearly demonstrate that the fluorescence reporter expression responds to changes in bona fide pri-miRNA processing activity, can detect the processing potential of mutant pri-miRNA, and reflects the function of ectopically expressed N-flag-DGCR8 proteins. The latter observation will be used to examine DGCR8 mutants.

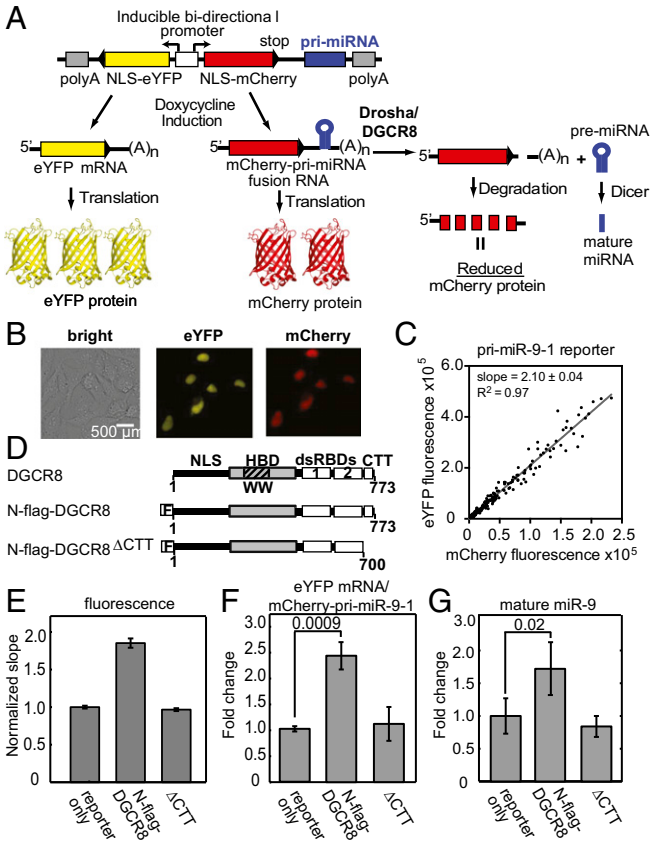

Fig. 1. Live-cell pri-miRNA processing reporter assay. (*A*) Schematic depiction of the assay. NLS, nuclear localization signal. (*B*) Exemplary cell images showing nuclear expression of eYFP and mCherry via transfection of the pri-miR-9-1 reporter. (*C*) eYFP and mCherry fluorescence signals from transfection with the pri-miR-9-1 reporter are plotted for each cell. Slope from a linear regression is shown on the graph, with $R^2 = 0.97$. (*D*) Schematics of human DGCR8 and the expression constructs used in the study. (*E*) Normalized fluorescence slopes for HeLa cells transfected with the pri-miR-9-1 reporter, either alone or with N-flag-DGCR8 expression plasmids. Error bars represent 95% confidence interval (95% CI) of the linear fit. The eYFP vs. mCherry scatter plots are in Fig. S1. (*F* and *G*) The abundance of the eYFP mRNA, the mCherry–pri-miRNA fusion RNA (*F*), and mature miR-9 (*G*) expression levels from *E* was measured using qRT-PCR (mean ± SD, $n = 3$). *P* values are labeled on the graphs.

The Reporter Assay Detects Alteration of Endogenous DGCR8 Activity. We next tested whether our reporter assay was sensitive to perturbation of DGCR8 expression via RNA interference. We

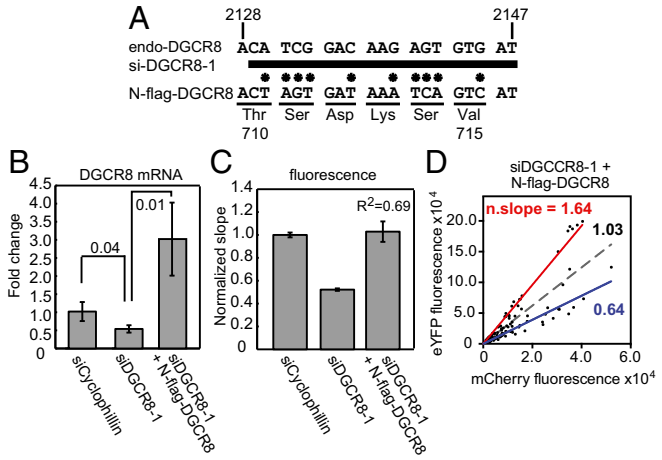

Fig. 2. The reporter assay detects alteration of endogenous DGCR8 activity. HeLa cells were cotransfected using Dharmafect duo with the pri-miR-9-1 reporter and siRNAs as indicated. Knockdown of endogenous DGCR8 was rescued via inclusion of pN-flag-DGCR8. (*A*) Schematic of the siDGCR8-1 binding site in the endogenous DGCR8 coding sequence. siDGCR8-1 is represented by the thick bar. Asterisks designate the location of mutations. (*B*) DGCR8 expression levels as measured using qRT-PCR. Shown are averages ± SD ($n = 3$). *P* values are labeled on the graph. (*C*) The mCherry vs. eYFP slopes (± 95% CI) normalized to siCyclophilin. The eYFP vs. mCherry scatter plots for cotransfections of pri-miR-9-1 reporter with either siCyclophilin or siDGCR8-1 are shown in Fig. S3 *A* and *B*, and that for the cotransfection of the reporter with siDGCR8-1 and pN-flag-DGCR8 is displayed in *D*. Dashed gray line is the linear regression for all data points. The red and blue lines are the linear regressions for the data points that lie above or below the dashed line, respectively. n. slope, normalized slope.

synthesized an siRNA, siDGCR8-1, that had been previously shown to reduce DGCR8 expression and decrease pri-miRNA processing and the abundance of mature miRNAs (10) (Fig. 2*A*). HeLa cells were cotransfected with siDGCR8-1 and the pri-miR-9-1 reporter. siCyclophilin was used as a normalization control. siDGCR8-1 reduced the expression of endogenous DGCR8 mRNA by 50% (Fig. 2*B*) and resulted in a 48% decrease in the fluorescence slope (Fig. 2*C*). This result indicates that our reporter is sensitive enough to detect a change in pri-miRNA processing efficiency caused by a modest reduction of endogenous DGCR8 expression. Note that the reduction of DGCR8 expression achieved here by RNA interference is similar to the ∼50% decrease observed in a DiGeorge syndrome mouse model (20, 21).

We also tested whether the pri-miRNA–processing defect caused by siDGCR8-1 could be rescued by expressing N-flag-DGCR8. siDGCR8-1 targets a coding sequence in the C-terminal region of endogenous DGCR8; the N-flag-DGCR8 expression plasmid (pN-flag-DGCR8) contains 10 silent mutations within the siDGCR8-1 targeting site so that siDGCR8-1 does not affect the expression of this exogenous DGCR8 (Fig. 2*A*). Cotransfection of pN-flag-DGCR8 with the reporter and siDGCR8-1 enhanced the total DGCR8 expression to three times the level of the siCyclophilin control (Fig. 2*B*) and resulted in an overall eYFP/mCherry slope twice that of siDGCR8-1 only (Fig. 2*C*). This result is consistent with a rescue of pri-miRNA processing by expression of N-flag-DGCR8. The siDGCR8-1/pN-flag-DGCR8 data have a large deviation from the fitted line, with an R^2 value of 0.69, much lower than the >0.86 values obtained from most other experiments (Figs. 2 *C* and *D*). In fact, there appeared to be two cell populations, which can be roughly separated by the fit curve (gray dashed line in Fig. 2*D*). The lower cell population has a normalized eYFP/mCherry slope of 0.64 ($R^2 = 0.89$), which is close to that of the siDGCR8-1, whereas the upper cell population displays a normalized slope of 1.64 ($R^2 = 0.97$), which is close to the slope of N-flag-DGCR8 overexpression, 1.90 (Figs. 2*D* and 1*E*). A control transfection with a fluorescein-labeled siRNA indicated that the siRNA got into most cells. Thus, it is likely that the lower cell population took up the reporter and siDGCR8-1 whereas the upper population received the reporter, pN-flag-DGCR8, and siDGCR8-1. This interpretation is supported by further experiments, in which the amount of pN-flag-DGCR8 used in the transfection was increased from 0.1 to 0.3 μg and the percentage of cells present in the upper population increased correspondingly (Fig. S3 *C* and *D*). These results demonstrate that a benefit of our fluorescence imaging-based assay is to allow pri-miRNA processing efficiency of different cell populations to be detected.

Overexpression of Drosha Does Not Enhance Pri-miRNA Processing. We showed that pri-miRNA processing is sensitive to both overexpression and RNAi knockdown of DGCR8. As Drosha and DGCR8 are known to function together, we compared the pri-miRNA processing efficiency of HeLa cells ectopically expressing either Drosha-flag, N-flag-DGCR8, or both. Fluorescence measurements showed that transfection of pCK-Drosha-flag did not increase processing activity, in contrast to the pN-flag-DGCR8 transfection; and coexpression of Drosha and DGCR8 resulted in pri-miRNA processing efficiency either higher than (pri-miR-9-1 reporter) or similar to (pri-miR-30a reporter) N-flag-DGCR8 expression alone (Figs. S4 *A* and *B* and S5 *A* and *B*). Similarly, mature miR-9 expression did not increase after Drosha-flag expression but did increase to threefold that of the reporter only after N-flag-DGCR8 expression, and to 6.8-fold after coexpression (Fig. S4*C*). qRT-PCR analyses indicate that Drosha expression was successful with its mRNA level doubled in the cotransfection with the pri-miR-9-1 reporter and quadrupled with the pri-miR-30a reporter (Figs. S4*E* and S5*D*). These changes are modest compared with the 45- to 85-fold increase observed for DGCR8 (Figs. S4*D* and S5*C*) but are comparable with the DGCR8 expression level achieved in the cotransfection with siDGCR8-1 where large changes in pri-miRNA processing efficiency were observed (Fig. 2). Overall, our results seem to suggest that, in HeLa cells, DGCR8, not Drosha, is the rate-limiting factor for pri-miRNA processing. This notion is consistent with the previous reports that the DGCR8 protein is subjected to multiple layers of regulation (5, 30, 33–36).

All Known Heme-Binding–Deficient DGCR8 Mutants Are Defective in Pri-miRNA Processing in HeLa Cells. We used our cellular assay to investigate the role of heme in DGCR8 function. Cys352 is conserved in all DGCR8 family members and serves as the coaxial ligand to the Fe(III) in heme (28). Mutation of Cys352 to an alanine, serine, or histidine residue completely abolishes heme binding to the NC1 protein and reduces its pri-miRNA processing activity in vitro. Therefore, we tested the C352A mutant to examine the importance of heme binding in live cells. We set up a series of cotransfections of the pri-miR-9-1 reporter with pN-flag-DGCR8, either wild type or the ΔCTT or C352A mutants. Compared with the wild type, we observed a 51% decrease in the eYFP/mCherry fluorescence slope for the C352A transfection, which corresponds to a decrease in the processing activity (Fig. 3*A*). Similarly, the eYFP/mCherry–pri-miRNA fusion RNA ratio and the mature miR-9 level decreased in the C352A transfection (Fig. 3 *B* and *C*). In contrast, the fluorescence slope, the mCherry–pri-miR-9-1 fusion RNA and mature miR-9 levels for C352A are very similar to those for the inactive ΔCTT (Fig. 3 *A*–*C*). Furthermore, C352A was expressed at a similar level as the wild type, as shown by Western blotting (Fig. 3*D*). Thus, the lack of pri-miRNA processing activity observed for C352A is not due to reduced expression of the mutant protein. Altogether, these results clearly indicate that the DGCR8 C352A mutant is inactive in pri-miRNA processing in HeLa cells.

We subsequently tested additional heme-binding–deficient DGCR8 mutants. The crystal structures of the DGCR8 dimerization domains show that Cys352 and Trp329 cluster on a putative heme-binding surface (27, 37). Mutation of Trp329 to either alanine (the residue at the equivalent position in fly Pasha)

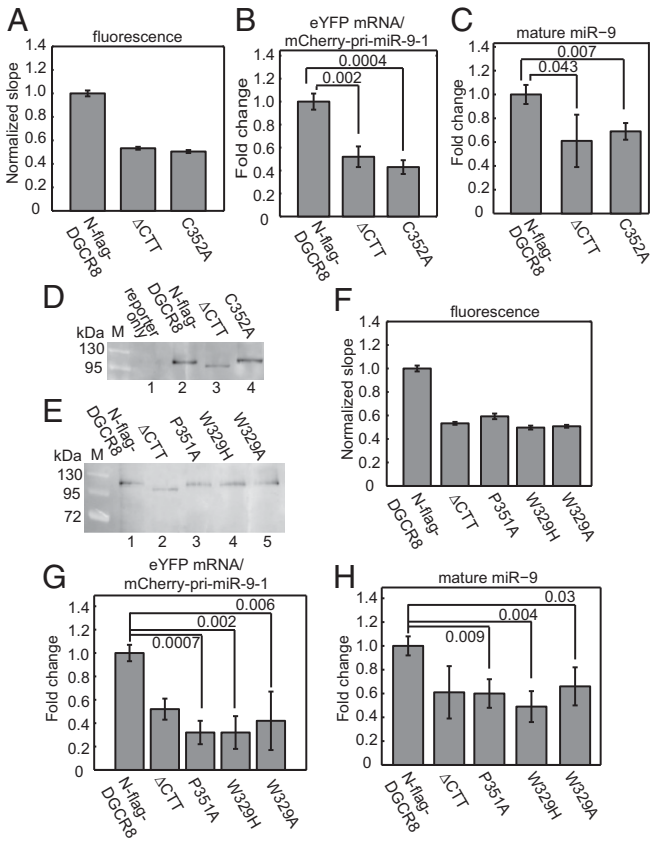

Fig. 3. All known heme-binding–deficient point mutants of DGCR8 are defective in pri-miRNA processing. HeLa cells were cotransfected with the pri-miR-9-1 reporter and N-flag-DGCR8 expression plasmids as indicated. (*A*) The normalized eYFP/mCherry slope (± 95% CI) of N-flag-DGCR8 C352A. (*B* and *C*) qRT-PCR analyses (mean ± SD, $n = 3$) of the (*B*) mCherry–pri-miRNA fusion RNA and (*C*) the mature miR-9 of the cotransfections in *A*. (*D* and *E*) Anti-flag immunoblots with equal amounts of nuclear extracts loaded. (*F*) Normalized fluorescence slopes (± 95% CI) for transfections with the DGCR8 mutants. (*G* and *H*) qRT-PCR analyses of (*G*) mCherry–pri-miRNA fusion RNA and (*H*) mature miR-9 for the transfections in *F*. Error bars represent SD ($n = 3$). *P* values are labeled on the graphs. The eYFP vs. mCherry fluorescence scatter plots are shown in Fig. S6 *A–D*.

or histidine (the residue in worms) in NC1 results in heme-free proteins after overexpression; and both mutants have reduced pri-miRNA processing activity in vitro (27). In addition to Trp329, Pro351 is also important for DGCR8 heme binding. Mutation of Pro351 to Ala greatly reduces the affinity of DGCR8 for heme (28). We therefore tested the activity of P351A, W329A, and W329H using our cellular pri-miRNA processing assay. In our initial experiments, equal amounts of wild-type and mutant plasmids were used in transfections; however, the three mutant proteins were expressed at slightly lower levels than the wild type. Thus, we doubled the amounts of the mutant plasmids in the transfections and achieved protein expression levels nearly equal to that of the wild type (Fig. 3*E*). Under the latter condition, all three mutants displayed normalized fluorescence slopes and eYFP/mCherry–pri-miR-9-1 fusion RNA ratios significantly lower than that of N-flag-DGCR8 but similar to ΔCTT (Fig. 3 *F* and *G*). Mature miR-9 levels decreased an average of 50% for all mutants relative to the wild type, again similar to that of ΔCTT (Fig. 3*H*). We tested these heme-binding–deficient mutants using the pri-miR-30a reporter construct and obtained similar results (Fig. S6 *E–K*). Altogether, these data clearly demonstrate that all known heme-binding–deficient DGCR8 mutants are defective in pri-miRNA processing in HeLa cells.

An "IPCL" Motif Is Required for Heme Binding and for Pri-miRNA Processing. The unique properties of DGCR8 encouraged us to search for motifs that are important for heme binding. The residues in the vicinity of Pro351 and Cys352 show a high degree of conservation among DGCR8 family members (Fig. 4*A*). Ile350 and Leu353 are invariable, Ser349 is conserved except in shrimp and insects, and His354 is conserved except in shrimp, insects, and worms. We mutated Ser349, Ile350, Leu353, and His354 to alanine in the context of NC1 and examined their heme-binding properties through overexpression in *E. coli* and purification using our routine procedures. The I350A and L353A mutations nearly abolished the presence of heme in purified NC1 proteins, and the mutant heme-free proteins cannot bind heme in vitro to reconstitute the complexes (Fig. S7 and Table S1). In contrast, purified S349A and H354A NC1 dimer proteins were occupied by heme, resembling the wild type. We then introduced these mutations to pN-flag-DGCR8 and tested their activity using the pri-miR-9-1 reporter. We found that S349A and H354A were active and that I350A and L353A were inactive in HeLa cells, as judged by the eYFP/mCherry fluorescence ratios (Fig. 4*B* and Fig. S8) and mature miR-9 levels (Fig. 4*C*). All DGCR8 point mutants were expressed at roughly equal levels as determined by qRT-PCR except for L353A, which had a higher expression level similar to the ΔCTT mutant (Fig. 4*D*). The nearly perfect correlation between heme binding, pri-miRNA processing, and sequence conservation observed in our mutagenesis analyses strongly supports an essential function of heme in the miRNA maturation pathway in animals.

Heme Availability and Biosynthesis in HeLa Cells Affects Pri-miRNA Processing. We tested whether cellular heme availability affects pri-miRNA processing activity using our cellular reporter assay. We cultured HeLa cells in heme-depleted media and compared their pri-miRNA processing efficiency with and without 10 μM hemin as supplement. The eYFP/mCherry fluorescence slope for cells grown under the heme-replenished condition had a modest but statistically significant increase (normalized slope = 1.11, $P = 0.0012$), which indicates an increase in pri-miRNA processing efficiency (Fig. 5*A*). Importantly, the mature miR-9 level nearly

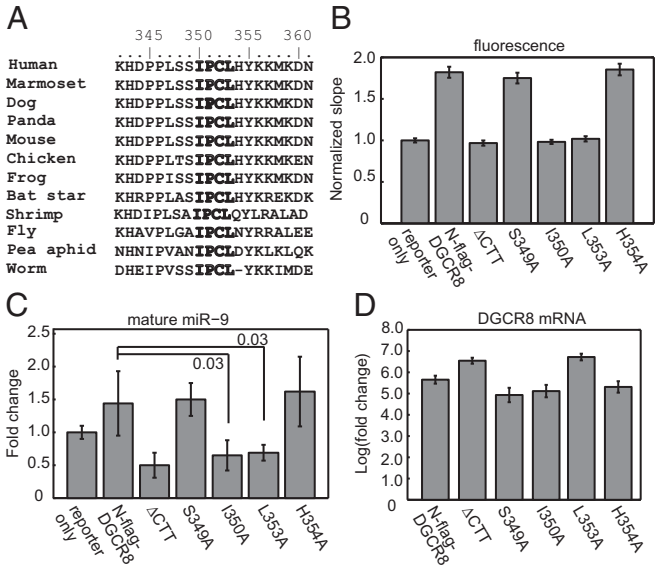

Fig. 4. The IPCL heme-binding motif is required for pri-miRNA processing. (*A*) Sequence alignment of DGCR8 homologs. (*B*) HeLa cells were cotransfected with the pri-miR-9-1 reporter and N-flag-DGCR8 expression plasmids as indicated. The normalized mCherry/eYFP slopes (± 95% CI) are shown. The eYFP vs. mCherry scatter plots are shown in Fig. S8. (*C*) qRT-PCR analyses (mean ± SD, $n = 3$) of mature miR-9 expression and (*D*) DGCR8 expression. *P* values are labeled on the graphs.

doubled in the presence of hemin, suggesting that alteration in heme availability in cellular environments can make large differences in mature miRNA levels (Fig. 5*B*). We also measured the amount of newly synthesized heme and observed a 60% reduction upon hemin treatment (Fig. 5C). This result is not surprising, as heme biosynthesis is known to be regulated via a feedback mechanism. Measurements of eYFP mRNA levels suggest that increase in miR-9 abundance by hemin was not caused by an enhanced rate of transcription (Fig. 5*D*).

We next examined the effects of inhibiting endogenous heme biosynthesis on pri-miRNA processing. We cultured HeLa cells under the heme-depleted condition, as described above, and treated them with 1 mM succinylacetone (SA). SA is a cell-permeable inhibitor of aminoluvelinic acid dehydratase, an enzyme responsible for the second step in the heme biosynthesis pathway (38). In a parallel experiment, the heme deficiency was rescued via addition of 10 μM hemin. To reduce secondary effects, we limited the duration of heme biosynthesis inhibition to 10 h. SA effectively reduced the amount of newly synthesized heme to about 25% that of no-treatment cells (Fig. 5*C*) and resulted in a 12% decrease in the eYFP/mCherry fluorescence slope, which corresponds to a decrease in pri-miRNA processing activity (Fig. 5*A*). The addition of SA did not decrease the levels of mature miR-9 compared to that with no treatment (Fig. 5*B*). However, we observed an increase in eYFP mRNA level after SA treatment, which suggests that the mCherry–pri-miR-9 transcription is likely to have increased under this condition (Fig. 5*D*). The lack of change in miR-9, despite the increased pri-miR-9-1 transcription, suggests that processing efficiency decreased after SA treatment. The lack of changes in miR-9 could also be contributed by a reduction of cell growth, an effect known to associate with inhibition of heme biosynthesis (39). The addition of exogenous hemin along with SA reversed the change in eYFP/mCherry fluorescence slope to a 17% increase relative to SA-treated cells (Fig. 5*A*), and the abundance of mature miR-9 doubled relative to those under both no-treatment and SA conditions (Fig. 5*B*). Because the changes of pri-miRNA processing efficiency caused by hemin and SA treatments were relatively small, we repeated these experiments and analyzed the RNAs using Northern blots. The trends in mature miR-9 levels were confirmed (Fig. S9*E*). Additionally, we observed an increase of the mCherry–pri-miR-9-1 fusion RNA upon SA treatment, which was reversed by hemin (Fig. S9*E*). Based on these observations, we conclude that both heme availability from extracellular environments and endogenous heme biosynthesis positively affect pri-miRNA processing. These effects are most likely to be exerted via the DGCR8–heme interaction. As the reduced pri-miRNA processing caused by inhibition of endogenous heme biosynthesis can be rescued by addition of hemin to the media, the origin of heme does not seem to be critical.

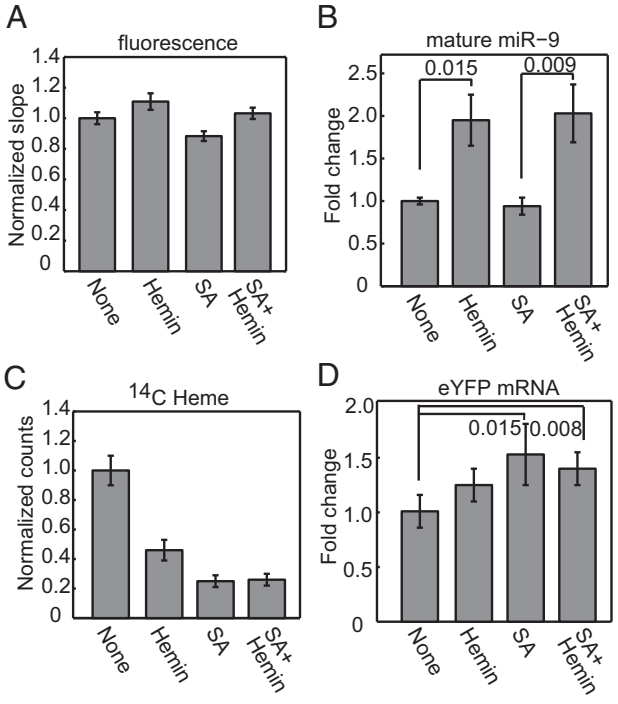

Fig. 5. Heme availability and biosynthesis in cells affects pri-miRNA processing. HeLa cells, grown in heme-depleted media and transfected with the pri-miR-9-1 reporter, were treated for 10 h with either hemin (10 μM) or succinylacetone (1 mM) or both. (*A*) Normalized eYFP/mCherry fluorescence slopes (± 95% CI). The eYFP vs. mCherry scatter plots are shown in Fig. S9 *A–D*. (*B*) Mature miR-9 expression (mean ± SEM, $n = 7$). (*C*) HeLa cells were treated with ^{14}C-labeled aminolevulinic acid, heme was extracted, and the radioactivity was measured. Measurements were normalized to the no-treatment (none) condition (mean ± SD, $n = 3$). (*D*) qRT-PCR analyses of eYFP expression (mean ± SD, $n = 4$). *P* values are labeled on the graphs.

Discussion

Here, we present a robust cellular assay for monitoring pri-miRNA cleavages. The assay is sensitive to both ectopic expression and RNA interference of the pri-miRNA processing machinery and thus can detect both increases and decreases in processing efficiency. The use of single-cell analyses and normalization with eYFP results in a sensitive and accurate reporter. Our assay enables us to isolate pri-miRNA processing efficiency from complex biological processes and diseases. With this technical advance, a multitude of questions about the Microprocessor complex could be investigated, including regulation of the Microprocessor and structural features of pri-miRNAs required for efficient processing (40, 41).

Using this assay we have analyzed the function of heme in miRNA maturation. Through a series of mutagenesis, we found that the six heme-binding–deficient DGCR8 mutants are defective in pri-miRNA processing. This correlation between heme binding and pri-miRNA processing in DGCR8 strongly argues for an essential function of heme in miRNA maturation. This conclusion is further strengthened by the observation that hemin activates pri-miRNA processing in HeLa cells cultured in heme-depleted media; and a heme biosynthesis inhibitor decreases processing. Because the heme-binding residues are highly conserved in animals (37), we speculate that the heme is also required in DGCR8 homologs.

We identified a previously uncharacterized heme-binding motif, IPCL. This motif shares similarity to the heme regulatory motif (HRM), which contains Cys-Pro, but in the opposite order. HRM directly binds heme and is found in repeats in a range of heme- regulated proteins such as the yeast transcription activator HAP1, the human δ-aminolevulenic acid synthase, and heme oxygenase-2 (42). It is possible that, in both motifs, the proline helps position the cysteine side chain in an appropriate geometry for ligation and for catalytic or regulatory functions. The conserved motif IPCL is essential but not sufficient for DGCR8 to associate with heme, as the dimerization subdomain, including Trp329 in the WW motif, and the C-terminal region of the HBD are also required for high-affinity association with heme. A bioinformatics search of protein sequences that contain both WW motif and IPCL yielded only DGCR8 homologs.

We show that heme is necessary for DGCR8 activity in live cells. What is the function of the DGCR8–heme interaction? There are two major possibilities that are not mutually exclusive. First, DGCR8 may be directly regulated by the availability of heme (43). In support of this possibility, we have shown previously that Fe(III) heme, but not the Fe(II) form, activates the pri-miRNA processing activity of DGCR8 in vitro (34) and here that heme availability and biosynthesis affect pri-miRNA processing efficiency in HeLa cells. Furthermore, heme oxygenase-1 (HO-1) was shown to reduce the total pool of cellular mature miRNAs and pre-miRNAs, in addition to blocking the induction of muscle-specific miRNA in myoblasts (44). HO-1 degrades heme in response to

various stress conditions. Although the increased miRNA level was attributed to decreases in DGCR8 protein levels, this observation is also consistent with reduced activation of the DGCR8 protein caused by increased heme degradation. As heme is synthesized in cells as the Fe(II) form, oxidation of the heme iron may also affect pri-miRNA processing.

The second possibility is that the heme bound to DGCR8 serves a structural purpose. We have shown that DGCR8 binds Fe(III) heme very tightly, making it hard to act as a reversible sensor of heme. Although the observation that reduction of the heme bound to DGCR8 to the Fe(II) state renders the protein inactive in pri-miRNA processing suggests a redox regulation, the reduction requires long incubation (30–60 min) with a strong reductant dithionite (34). Thus, reversible redox switch of the DGCR8-bound heme is unlikely to occur under physiological conditions. Additionally, the dual-cysteine ligation of the Fe(III) heme by DGCR8 makes the heme unavailable for potential catalytic functions. These hypotheses should be tested in the future.

Materials and Methods

Additional procedures can be found in *SI Materials and Methods*.

Vectors and Cloning. The pri-miRNA processing reporters were engineered based on the bidirectional tetracycline-inducible vector containing mCherry and eYFP (pTRE-BI-red/yellow) (29). Fragments of pri-miR-9-1 (143 nt) and pri-miR-30a (148 nt) were PCR-amplified from human genomic DNA and subsequently cloned into pTRE-BI-red/yellow.

Cell Culture and Transfection. The HeLa Tet-On cell line was purchased from Clontech. HeLa Tet-On cells were cultured in DMEM (Life Technologies) with 5% Tet-system approved FBS (Clontech) in 5% CO_2 at 37 °C. Cells were transfected with Effectene (Qiagen) following manufacturer's instructions.

Imaging and Analysis. All imaging was performed using a Nikon Eclipse Ti microscope equipped with an EMCCD camera (Andor iXon). We wrote a program based on the Matlab software package (The MathWorks) for integrating fluorescence intensities of individual cells, which is described in *SI Materials and Methods*.

ACKNOWLEDGMENTS. We thank P. Sharp for sharing the pTRE-BI-red/yellow plasmid long before publication, L. Zhang for advice on measurements of heme biosynthesis and for sharing ^{14}C-ALA, J. Feigon for sharing equipment, Y. Chen for technical support, and R. Senturia for sharing experience and discussion. This work was supported by National Institutes of Health Grants GM080563 (to F.G.), T32GM008496 (to S.H.W.), and GM069709 (to S.W.).

1. Ambros V (2011) MicroRNAs and developmental timing. *Curr Opin Genet Dev* 21(4): 511–517.
2. Guo H, Ingolia NT, Weissman JS, Bartel DP (2010) Mammalian microRNAs predominantly act to decrease target mRNA levels. *Nature* 466(7308):835–840.
3. Fabian MR, Sonenberg N, Filipowicz W (2010) Regulation of mRNA translation and stability by microRNAs. *Annu Rev Biochem* 79:351–379.
4. Kim VN, Han J, Siomi MC (2009) Biogenesis of small RNAs in animals. *Nat Rev Mol Cell Biol* 10(2):126–139.
5. Guo F (2012) *The Enzymes: Eukaryotic RNases and their Partners in RNA Degradation and Biogenesis, Part B*, eds Guo F, Tamanoi F (Elsevier Academic, Amsterdam), pp 101–121.
6. Lee Y, Jeon K, Lee J-T, Kim S, Kim VN (2002) MicroRNA maturation: Stepwise processing and subcellular localization. *EMBO J* 21(17):4663–4670.
7. Lee Y, et al. (2003) The nuclear RNase III Drosha initiates microRNA processing. *Nature* 425(6956):415–419.
8. Denli AM, Tops BBJ, Plasterk RHA, Ketting RF, Hannon GJ (2004) Processing of primary microRNAs by the Microprocessor complex. *Nature* 432(7014):231–235.
9. Gregory RI, et al. (2004) The Microprocessor complex mediates the genesis of microRNAs. *Nature* 432(7014):235–240.
10. Han J, et al. (2004) The Drosha-DGCR8 complex in primary microRNA processing. *Genes Dev* 18(24):3016–3027.
11. Landthaler M, Yalcin A, Tuschl T (2004) The human DiGeorge syndrome critical region gene 8 and its D. melanogaster homolog are required for miRNA biogenesis. *Curr Biol* 14(23):2162–2167.
12. Hutvágner G, et al. (2001) A cellular function for the RNA-interference enzyme Dicer in the maturation of the let-7 small temporal RNA. *Science* 293(5531):834–838.
13. Bernstein E, Caudy AA, Hammond SM, Hannon GJ (2001) Role for a bidentate ribonuclease in the initiation step of RNA interference. *Nature* 409(6818):363–366.
14. Blahna MT, Hata A (2013) Regulation of miRNA biogenesis as an integrated component of growth factor signaling. *Curr Opin Cell Biol* 25(2):233–240.
15. Croce CM (2009) Causes and consequences of microRNA dysregulation in cancer. *Nat Rev Genet* 10(10):704–714.
16. Suzuki HI, et al. (2009) Modulation of microRNA processing by p53. *Nature* 460(7254): 529–533.
17. Piskounova E, et al. (2011) Lin28A and Lin28B inhibit let-7 microRNA biogenesis by distinct mechanisms. *Cell* 147(5):1066–1079.
18. Davis BN, Hilyard AC, Lagna G, Hata A (2008) SMAD proteins control DROSHA-mediated microRNA maturation. *Nature* 454(7200):56–61.
19. Shiohama A, Sasaki T, Noda S, Minoshima S, Shimizu N (2003) Molecular cloning and expression analysis of a novel gene DGCR8 located in the DiGeorge syndrome chromosomal region. *Biochem Biophys Res Commun* 304(1):184–190.
20. Stark KL, et al. (2008) Altered brain microRNA biogenesis contributes to phenotypic deficits in a 22q11-deletion mouse model. *Nat Genet* 40(6):751–760.
21. Fénelon K, et al. (2011) Deficiency of Dgcr8, a gene disrupted by the 22q11.2 microdeletion, results in altered short-term plasticity in the prefrontal cortex. *Proc Natl Acad Sci USA* 108(11):4447–4452.
22. Rüegger S, Großhans H (2012) MicroRNA turnover: When, how, and why. *Trends Biochem Sci* 37(10):436–446.
23. Peric D, Chvalova K, Rousselet G (2012) Identification of microprocessor-dependent cancer cells allows screening for growth-sustaining micro-RNAs. *Oncogene* 31(16):2039–2048.
24. Tsutsui M, et al. (2008) Establishment of cells to monitor Microprocessor through fusion genes of microRNA and GFP. *Biochem Biophys Res Commun* 372(4):856–861.
25. Allegra D, Mertens D (2011) In-vivo quantification of primary microRNA processing by Drosha with a luciferase based system. *Biochem Biophys Res Commun* 406(4):501–505.
26. Faller M, Matsunaga M, Yin S, Loo JA, Guo F (2007) Heme is involved in microRNA processing. *Nat Struct Mol Biol* 14(1):23–29.
27. Senturia R, et al. (2010) Structure of the dimerization domain of DiGeorge critical region 8. *Protein Sci* 19(7):1354–1365.
28. Barr I, et al. (2011) DiGeorge critical region 8 (DGCR8) is a double-cysteine-ligated heme protein. *J Biol Chem* 286(19):16716–16725.
29. Mukherji S, et al. (2011) MicroRNAs can generate thresholds in target gene expression. *Nat Genet* 43(9):854–859.
30. Gong M, et al. (2012) Caspases cleave and inhibit the microRNA processing protein DiGeorge Critical Region 8. *Protein Sci* 21(6):797–808.
31. Faller M, et al. (2010) DGCR8 recognizes primary transcripts of microRNAs through highly cooperative binding and formation of higher-order structures. *RNA* 16(8):1570–1583.
32. Yeom K-H, Lee Y, Han J, Suh MR, Kim VN (2006) Characterization of DGCR8/Pasha, the essential cofactor for Drosha in primary miRNA processing. *Nucleic Acids Res* 34(16): 4622–4629.
33. Wada T, Kikuchi J, Furukawa Y (2012) Histone deacetylase 1 enhances microRNA processing via deacetylation of DGCR8. *EMBO Rep* 13(2):142–149.
34. Barr I, et al. (2012) Ferric, not ferrous, heme activates RNA-binding protein DGCR8 for primary microRNA processing. *Proc Natl Acad Sci USA* 109(6):1919–1924.
35. Han J, et al. (2009) Posttranscriptional crossregulation between Drosha and DGCR8. *Cell* 136(1):75–84.
36. Triboulet R, Chang H-M, Lapierre RJ, Gregory RI (2009) Post-transcriptional control of DGCR8 expression by the Microprocessor. *RNA* 15(6):1005–1011.
37. Senturia R, Laganowsky A, Barr I, Scheidemantle BD, Guo F (2012) Dimerization and heme binding are conserved in amphibian and starfish homologues of the microRNA processing protein DGCR8. *PLoS ONE* 7(7):e39688.
38. Ebert PS, Hess RA, Frykholm BC, Tschudy DP (1979) Succinylacetone, a potent inhibitor of heme biosynthesis: Effect on cell growth, heme content and δ-aminolevulinic acid dehydratase activity of malignant murine erythroleukemia cells. *Biochem Biophys Res Commun* 88(4):1382–1390.
39. Ye W, Zhang L (2004) Heme deficiency causes apoptosis but does not increase ROS generation in HeLa cells. *Biochem Biophys Res Commun* 319(4):1065–1071.
40. Han J, et al. (2006) Molecular basis for the recognition of primary microRNAs by the Drosha-DGCR8 complex. *Cell* 125(5):887–901.
41. Zeng Y, Cullen BR (2005) Efficient processing of primary microRNA hairpins by Drosha requires flanking nonstructured RNA sequences. *J Biol Chem* 280(30):27595–27603.
42. Zhang L, Guarente L (1995) Heme binds to a short sequence that serves a regulatory function in diverse proteins. *EMBO J* 14(2):313–320.
43. Mense SM, Zhang L (2006) Heme: A versatile signaling molecule controlling the activities of diverse regulators ranging from transcription factors to MAP kinases. *Cell Res* 16(8):681–692.
44. Kozakowska M, et al. (2012) Heme oxygenase-1 inhibits myoblast differentiation by targeting myomirs. *Antioxid Redox Signal* 16(2):113–127.

Supporting Information

Weitz et al. 10.1073/pnas.1309915111

SI Text

Determining Processing Competency of Pri-miRNAs in Cells. We tested whether the reporter assay can distinguish a processing-incompetent primary transcript of microRNA (pri-miRNA) mutant from the wild type. Pairing interaction around the Drosha cleavage sites in pri-mRNAs has been shown to be critical for processing (1). We mutated four residues around the 5′ Drosha cleavage site in the pri-miR-9-1 reporter to generate the M1 construct (Fig. S4*A*). Cotransfection of the M1 reporter with pN-flag-DGCR8 did not show the large increase in slope that was observed for the wild type (Fig. S4 *B* and *C*). Cotransfection with ΔCTT also did not exhibit significant changes. The lack of changes in processing of pri-miR-9-1 M1 by ectopic expression of N-flag-DGCR8 was confirmed by measurements of mCherry–pri-miR-9–1 fusion and eYFP mRNA levels using quantitative RT-PCR (qRT-PCR) (Fig. S4*D*). These results indicate that our reporter assay detects legitimate pri-miRNA cleavage events and may be used to examine processing competency of pri-miRNAs in cells.

SI Materials and Methods

Reagents. Succinylacetone (synonym 4,6-Dioxoheptanoic acid), doxycycline, and horse skeletal muscle apomyoglobin were from Sigma-Aldrich. Hemin was from MP Biomedicals. δ-Aminolevulinic acid (δ-ALA) was from either MP Biomedicals or Frontier Scientific. The siRNAs were purchased from Dharmacon, Thermo Scientific. The 4-^{14}C-aminolevulinic acid was a gift from Li Zhang (University of Texas at Dallas). Mature miR-9 Locked Nucleic Acids (LNA) probe was obtained from Exiqon.

Vectors and Cloning. The pri-miRNA processing reporters were engineered based on the bidirectional tetracycline-inducible vector containing mCherry and eYFP (pTRE-BI-red/yellow), both fused to an N-terminal nuclear localization signal sequence (2). Fragments of pri-miR-9-1 (143 nt) and pri-miR-30a (148 nt) were PCR-amplified from human genomic DNA. The primers were as follows with the ClaI and NotI cloning sites underlined: pri-miR-9-1 forward (ACCATCGATGGCTGCGTGGAAGAGGCGG), pri-miR-9-1 reverse (TGCAGCGGCCGCCTGCAGCCCCTCTGCGCAGT), pri-miR-30a forward (ACCATCGATGGAAAGAAGGTATATTGCT), pri-miR-30a reverse (TGCAGCGGCCGCAAACAAGATAATTGCTCCT).

The amplified pri-miRNAs were initially cloned into the ptre2hyg-HA vector (Clontech) between the ClaI and NotI sites for the purpose of a different study. The pri-miRNAs were subsequently excised using ClaI and SalI and inserted into pTRE-BI-red/yellow. The pri-miR-9-1 M1 mutant was made using the QuikChange site-directed mutagenesis protocol (Qiagen). Mutagenesis of N-flag-DGCR8 and NC1 expression constructs was carried out using the standard four-primer PCR method. The RNA- and protein-coding sequences of all plasmids were confirmed by sequencing.

Cell Culture and Transfection. The HeLa Tet-On cell line was purchased from Clontech. HeLa Tet-On cells were cultured in DMEM (Life Technologies) with 5% Tet-system approved FBS (Clontech) in 5% CO_2 at 37 °C. For transfections without siRNAs, 4.8×10^5 cells were seeded on 35-mm glass-bottom plates. The following day, cells were transfected with 0.4 μg of total DNA or 0.8 μg for low expression constructs using the Effectene reagent (Qiagen). Cells were immediately induced with 2 μg/mL doxycycline and imaged 18–24 h later unless specified otherwise. Media with phenol red were used for transfection and induction and were exchanged for a clear medium without the dye and containing 2 μg/mL doxycycline immediately before imaging.

Cotransfection of reporter and siRNAs was performed using the DharmaFECT Duo transfection reagent (Thermo Scientific) following the manufacturer's instructions. The final concentrations of siRNA and plasmid were 100 nM and 2 μg/mL, respectively. The sequence of siDGCR8-1 was the same as reported by Kim and coworkers (3). Cells were passaged 1 d posttransfection, plated on 35-mm glass-bottom plates, and 4 h later induced with 2 μg/mL doxycycline. Cells were imaged 18–24 h postinduction.

Heme-depleted media was made by treating Tet-system approved FBS with 0.1 M ascorbic acid for 2 h (4). The absorbance spectrum of the FBS was recorded at the beginning and throughout the treatment to monitor the disappearance of the 405-nm heme peak. The ascorbic acid was removed by dialyzing against 1 L of phosphate buffered saline (PBS, containing 137 mM NaCl, 2.7 mM KCl, 10 mM Na_2HPO_4, and 1.8 mM KH_2PO_4) at room temperature using dialysis tubing with a molecular mass cutoff of 12,500 Da twice for 1 h each round. Heme-depleted FBS was added to DMEM, and the medium was sterile-filtered. Cells were cultured in heme-depleted media for 24 h and split into either six-well plates or glass-bottom imaging plates. For pri-miRNA processing reporter assays, cells were transfected with Effectene. Either 1 mM succinylacetone (dissolved in water), 10 μM hemin (dissolved in DMSO), or both was added to the cell cultures at the same time as doxycycline. After 10 h, cells were either imaged or lysed for RNA extraction.

Measuring Rates of Heme Biosynthesis. To measure reduction in heme synthesis during succinylacetone/heme treatments, we added to the media 0.4 μCi of 4-^{14}C-aminolevulinic acid and 20 μM unlabeled δ-ALA. After 10 h, cells were washed twice with PBS, scraped into a 2-mL tube, and spun down at 13,226 × *g* for 1 min. Cells were resuspended in 0.3 mL of heme extraction buffer containing 80% (vol/vol) acetone and 0.5 M HCl. Then, 1.2 mL of diethyl ether was added, and the cells were spun down at 13,226 × *g* for 5 min at 4 °C. Two additional rounds of extraction with 2 M HCl were performed, and the final aqueous layer was added to a scintillation vial and allowed to evaporate overnight. The following day, 5 mL of scintillation fluid was added, and the amounts of ^{14}C-labeled heme were measured using a Beckman LS6500 liquid scintillation counter. Three biological replicates were performed, and the counts were normalized to the average of "no-treatment" samples.

Imaging and Analysis. All imaging was performed using a Nikon Eclipse Ti microscope equipped with an EMCCD camera (Andor iXon). We used a 20× air objective (NA = 0.45, Olympus) and lamp illumination (Nikon) at full power, an exposure time of 100 ms and 0 gain. The fluorescence signal was detected using filter cubes for eYFP (510 ± 10 nm band pass excitation and 535 ± 15 nm band pass emission) and mCherry (535 ± 25 nm band pass excitation and 610 ± 10 nm band pass emission). Images were saved as 16-bit tiff files.

We wrote a program based on the Matlab software package (The MathWorks) for integrating fluorescence intensities of individual cells. To determine the perimeter of individual nucleus (segmentation), our program imports individual pairs of eYFP and mCherry images and converts them to binary maps using user-defined threshold values. A value of 1 in the map indicates that the pixel is inside the nucleus, and 0 indicates outside. We

usually choose threshold values that maximize the number of cells detected. The perimeter of the nucleus is determined for each image separately, and then an adequate perimeter is chosen for the two images based on the following criteria. If the same cell is found in both images, the smaller perimeter is chosen to avoid including cytosols, which sometimes have low fluorescent signals. If a cell is detected in only one image, the perimeter is kept, allowing for very dim cells that are not detected in both images to be included. The center of the final perimeter for each cell is determined. After the nuclear perimeters are determined, further analysis is done on the original images. A background fluorescence value is calculated for each image by averaging the intensities of the pixels outside the identified nuclei. The background is then subtracted from the intensities of all pixels. The total intensity of an individual cell is calculated as the sum of the pixel intensities within the perimeter. Users can use the center coordinates in the output to remove dead cells or multiple cells detected as one object.

A list of total eYFP and mCherry intensities for individual cells was compiled in Microsoft Excel. Scatter plots were made for eYFP versus mCherry signals. The data were sorted based on each point's distance from the origin. Ten percent of the data with the highest intensities were removed, as they tend to dominate and possibly skew the linear fit. The final datasets were imported into Matlab and fit using the curve fit toolbox. *P* values were determined using the linear fit function of PRISM (GraphPad, version 4).

qRT-PCR for RNA Analyses. Total RNAs were extracted using the miRNeasy Mini kit (Qiagen) and were digested on-column using the RNase-free DNase set (Qiagen). The reverse transcription (RT) reactions were set up using SuperScript II (Life Technologies), and the quantitative PCR (qPCR) was performed using Platinum SYBR Green qPCR Supermix-UDG (Life Technologies). Following are a list of primers used for RT and qPCR reactions: mCherry RT (*TGTCAGGCAACCGTATTCACC*GTTCGTACTGTTCCACGA), eYFP RT (*TGTCAGGCAACCGTATTCACC*ACTCCAGCAGGACCATGTGAT), mCherry qPCR forward (ACTACGACGCTGAGGTCAA), eYFP qPCR forward (AAGATCCGCCACAACATCGA), and qPCR reverse for mCherry and eYFP (*TGTCAGGCAACCGTATTCACC).*

To prevent potential plasmid in the RNA samples from interfering with the qPCR reactions, the RT primers were designed to include a 21-nt 5′-overhang (shown above in italics). The qPCR reverse primer sequence was identical to this overhang whereas the forward primers were gene-specific. A three-step qPCR reaction was performed with an annealing temperature of 60 °C. qPCR results were analyzed using the MxPro software (Stratagene). We calculated the ΔC_t values of the mCherry and eYFP transcripts and determined the fold changes by normalizing to the reporter only control.

Mature miR-9 and miR-30a (miR-9-5p and miR-30a-5p in the current miRBase nomenclature) were detected using TaqMan miRNA reverse transcription and miRNA Assay kits (Life Technologies) following the manufacturer's instructions. Ten nanograms of total RNA was used in each reverse transcription. C_t values were subtracted by those of either U6 small nuclear RNA or β-actin mRNA. Fold changes were calculated and normalized to the reporter-only control. DGCR8 expression was detected using a Taqman gene expression assay (Life Technologies), with RT performed using a random primer set and SuperScipt II (Life Technologies). The C_t values were subtracted by those of β-actin mRNA, and the fold change was calculated and was normalized to that of the siCyclophillin control transfection. All *P* values were calculated using a two-tailed Student *t* test except in Fig. 2*B* where a one-tailed *t* test was used.

Northern Blotting. Total RNA samples were prepared using the TriZol reagent (Invitrogen) according to the manufacturer's instructions. RNA quality and relative concentrations were determined using 1% agarose gels. Three to 20 μg of RNAs were loaded onto 15% polyacrylamide gels containing 7 M urea and separated by electrophoresis. RNA was transferred to Hybond-N+ membranes (GE Healthcare) and was cross-linked using UV light. The probe for U6 snRNA is a DNA oligo with the sequence 5′-AACGCTTCACGAATTTGCGT-3′. The probes were 5′-labeled with γ-^{32}P- ATP and were hybridized to membranes in ULTRAhyb-Oligo hybridization buffer (Life Technology) at 42 °C overnight. The membranes were washed and exposed to phosphorimagers. The images were recorded using a Typhoon Variable Mode Imager, and the bands were quantified using the program Quantify One (version 4.4.1; Bio-Rad). The plotting was performed using the program PRISM (version 4.0; GraphPad).

Immunoblotting. HeLa cells were transfected with the wild-type and mutant pN-flag-DGCR8 plasmids using Effectene (Qiagen) following standard protocol. Twenty-four hours posttransfection, cells were washed twice with PBS, scraped into 200 μL of PBS, and pelleted by centrifugation at 1,000 × *g* for 2 min at 4 °C. The PBS was removed, and ∼1×10^6 cells were resuspended in 80 μL of cold Buffer A [10 mM Hepes-KOH (pH 7.9), 1.5 mM $MgCl_2$, 10 mM KCl, 0.5 mM DTT, 0.2 mM phenylmethylsulfonyl fluoride (PMSF)]. Cells were incubated on ice for 10 min and then vortexed for 10 s and pelleted by centrifugation at 16,000 × *g* for 10 s at 4 °C. The supernatant (cytoplasmic fraction) was transferred to a new tube. The pellet was resuspended in 50 μL of Buffer C [20 mM Hepes-KOH (pH 7.9), 25% glycerol, 420 mM NaCl, 1.5 mM $MgCl_2$, 0.5 mM DTT, 0.2 mM PMSF] and incubated on ice for 20 min. Cells were pelleted by centrifugation at 16,000 × *g* for 2 min at 4 °C. The supernatant (nuclear fraction) was transferred to a new tube and processed for immunoblotting following our standard procedure (5). The membranes were first incubated overnight with mouse anti-FLAG antibodies (Sigma; diluted 1:1,000) followed by a 2-h incubation at room temperature with anti-mouse antibodies conjugated with horseradish peroxidase (HRP) (Novagen) (1:30,000 dilution). The membrane was washed thoroughly in PBST (PBS with 0.2% Tween-20), and the ECL Plus Western Blotting Detection System (GE Healthcare) protocol was then used according to the manufacturer's instructions. The images were recorded using chemifluorescence and the Typhoon Variable Mode Imager (GE Healthcare).

Expression, Purification, and Characterization of Recombinant NC1 Proteins. Human NC1 (wild type and mutants) proteins were expressed and purified as previously described (6). Briefly, they were expressed in *Escherichia coli* BL21(DE3) CodonPlus cells (Stratagene) grown in LB media supplemented with 1 mM δ-ALA at the time of induction. These proteins were purified using cation exchange followed by size exclusion chromatography. The purified proteins were stored in a buffer containing 20 mM Tris, pH 8.0, 400 mM NaCl, and 1 mM DTT. Electronic absorption spectra were recorded on a Beckman-Coulter DU800 spectrophotometer at 25 °C.

Heme dissociation and association assays were performed as described (7), in a buffer containing 20 mM Tris, pH 8.0, 400 mM NaCl, and 1 mM DTT. Fe(III) heme-bound NC1 S349A and H354A mutants, at 5.75 and 4.0 μM dimer concentrations, respectively, were incubated at room temperature with eightfold molar excess of apomyoglobin, which has an extremely high affinity for heme, with K_D of 3×10^{-15} M, and serves as a heme sink. Electronic absorption spectra were recorded over a period of 24 h. No heme transfer from NC1 mutants to apomyoglobin was observed. For heme association with the heme-free NC1 mutant dimers, I350A and L353A, 5 μM of the proteins were titrated with up to 10 μM Fe(III) heme, and electronic absorption spectra were recorded. Hemin chloride was converted to Fe(III) heme by dissolving it in 1.4 M NaOH at 10 mM concentration and incubating in the dark at room temperature for >30 min.

This concentrated solution was then diluted in water to give a 100-μM stock solution. No absorption peaks were observed around 450 nm, where the signature DGCR8-Fe(III) heme Soret peak is located.

Sequence Alignment. The following National Center for Biotechnology Information (NCBI) accession numbers were used for the DGCR8 homolog alignment: Human, *Homo sapien* (NCBI accession no. NM_022720); Marmoset, *Callithrix jacchus* (XM_002806547); Dog, *Canis familiaris* (XM_543542.4); Panda, *Ailuropoda melanoleuca* (XM_002920581); Mouse, *Mus musculus* (NM_033324); Chicken, *Gallus gallus* (XM_415079); Frog, *Xenopus laevis* (BC070985); Bat star, *Patiria miniata* (GQ397480.1); Shrimp, *Litopenaeus vannamei* (HQ692889.1); Fly, *Drosophila melanogaster* (NM_143622); Pea aphid, *Acyrthosiphon pisum* (NW_003383706.1); and Worm, *Caenorhabditis elegans* (NM_060373).

1. Lee Y, et al. (2003) The nuclear RNase III Drosha initiates microRNA processing. *Nature* 425(6956):415–419.
2. Mukherji S, et al. (2011) MicroRNAs can generate thresholds in target gene expression. *Nat Genet* 43(9):854–859.
3. Han J, et al. (2004) The Drosha-DGCR8 complex in primary microRNA processing. *Genes Dev* 18(24):3016–3027.
4. Ye W, Zhang L (2004) Heme deficiency causes apoptosis but does not increase ROS generation in HeLa cells. *Biochem Biophys Res Commun* 319(4):1065–1071.
5. Gong M, et al. (2012) Caspases cleave and inhibit the microRNA processing protein DiGeorge Critical Region 8. *Protein Sci* 21(6):797–808.
6. Faller M, Matsunaga M, Yin S, Loo JA, Guo F (2007) Heme is involved in microRNA processing. *Nat Struct Mol Biol* 14(1):23–29.
7. Barr I, et al. (2011) DiGeorge critical region 8 (DGCR8) is a double-cysteine-ligated heme protein. *J Biol Chem* 286(19):16716–16725.

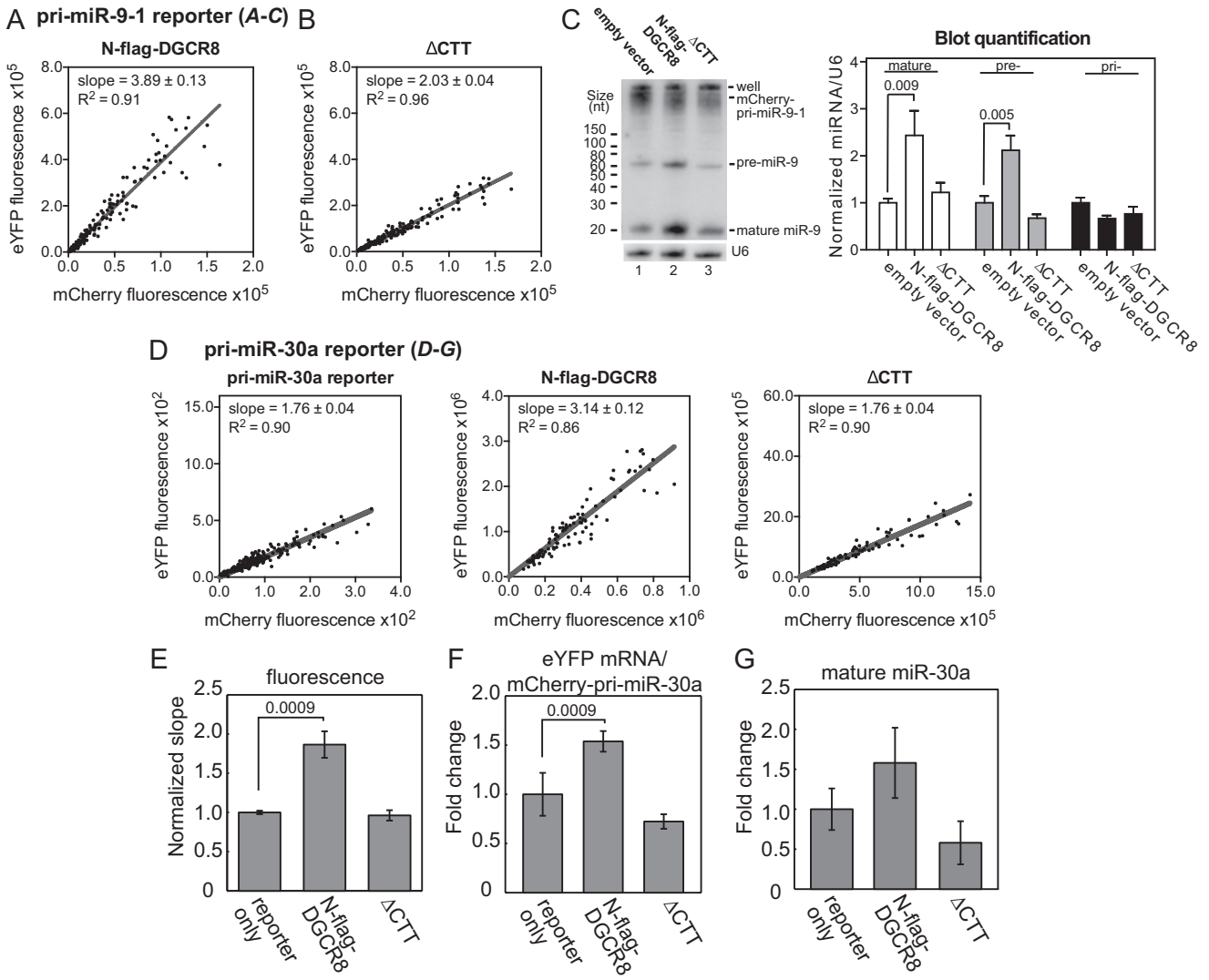

Fig. S1. Validation of the pri-miR-9–1 and pri-miR-30a reporters. (*A*–*C*) Validation of the pri-miR-9-1 reporter. Shown are additional data for the experiments described in Fig. 1*E*. Scatter plots of eYFP vs. mCherry fluorescent intensities of individual cells from cotransfection of the pri-miR-9-1 reporter with either wild-type N-flag-DGCR8 expression plasmid (*A*) or the ΔCTT mutant (*B*). The lines are from linear regression, with slope and R^2 shown on the graph. The ratio of *y* and *x* axes was set at 4:1 for all scatter plots. (*C*) Northern blotting analyses of total RNA samples. The pri-, pre-, and mature miR-9 intensities, after normalization by those of U6 snRNA, are indicated on the graph (mean ± SD, $n = 3$). (*D*–*G*) Validation of the pri-miR-30a reporter. HeLa cells were transfected with the pri-miR-30a reporter either alone or with N-flag-DGCR8 expression plasmid (wild type or ΔCTT). (*D*) Scatter plots of eYFP vs. mCherry fluorescence intensities of individual cells. The lines are from linear regression, with slope and R^2 shown on the graph. (*E*) Normalized eYFP/mCherry fluorescence slopes. Error bars represent 95% confidence interval (CI) of the linear fit. (*F* and *G*) qRT-PCR analyses of the mCherry-pri-miR-30a fusion RNA (*F*) and mature miR-30a (*G*). Error bars represent SD ($n = 3$). *P* values are labeled on the graphs.

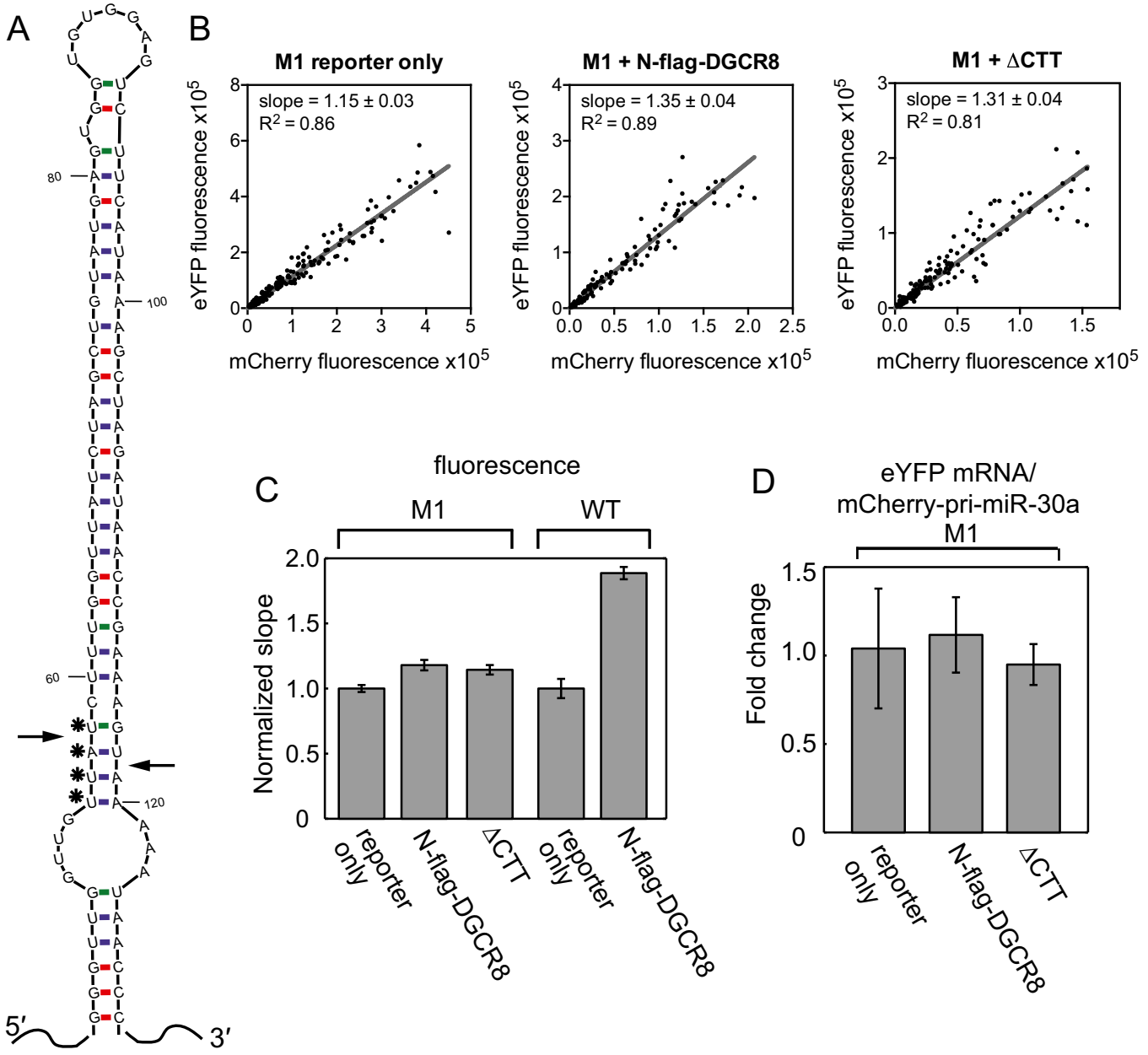

Fig. S2. Mutant pri-miR-9-1 reporter does not respond to ectopic expression of N-flag-DGCR8. (*A*) Secondary structure of the pri-miR-9-1 hairpin as predicted using MFOLD (1). Arrows indicate the expected Drosha cleavage sites. Residues marked by asterisks are mutated to AAUA (5′ to 3′) in the M1 mutant. (*B*) HeLa cells were transfected with the pri-miR-30a M1 or wild-type reporter, and pN-flag-DGCR8 plasmids as indicated. The eYFP and mCherry fluorescence signals are plotted for each cell. Slope and R^2 from linear regression are shown on the graph. The ratio of *y* and *x* axes was set at 1.6:1 for all plots. These experiments were performed together with those shown in Fig. 1*E*. (*C*) The normalized eYFP/mCherry fluorescence slopes are shown. Error bars are 95% CI from the linear fit. (*D*) qRT-PCR analyses of eYFP and mCherry-pri-miR-9-1 fusion RNAs from the experiments using the M1 reporter. Shown are average ± SD (n = 3). The slight changes, relative to the reporter-only control, are not statistically significant, with P value(N-flag-DGCR8) = 0.63 and P value(ΔCTT) = 0.93.

1. Zuker M (2003) Mfold web server for nucleic acid folding and hybridization prediction. *Nucleic Acids Res* 31(13):3406–3415.

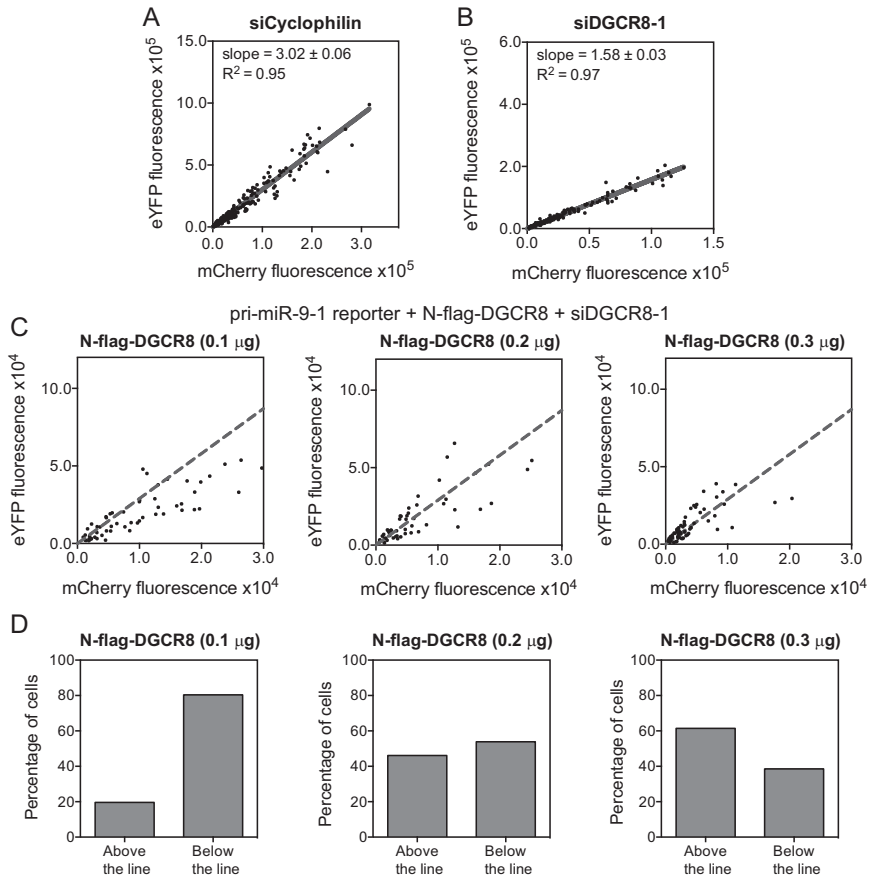

Fig. S3. Additional data to show that the reporter assay detects alteration of endogenous DGCR8 activity. (*A* and *B*) Scatter plots of eYFP vs. mCherry fluorescent intensities from the cotransfection of the pri-miR-9-1 reporter with siCyclophilin (*A*) or siDGCR8-1 (*B*), as described in Fig. 2*C*. The ratio of *y* and *x* axes was set at 4:1 for all scatter plots. (*C*) Scatter plots for cotransfections of the pri-miR-9-1 reporter, siDGCR8-1, and pN-flag-DGCR8. The amount of pN-flag-DGCR8 was varied whereas the amount of reporter was changed correspondingly to keep the total mass of plasmids to 0.4 μg, as required by the Effectene transfection protocol. The cells were assigned to the two groups based on the same gray dashed line as the linear regression fit for the data shown in Fig. 2*D* (slope = 2.9). (*D*) The percentage of data points that fell above and below the gray dashed line in *C*. We believe that cells above the line received pN-flag-DGCR8 whereas those below did not.

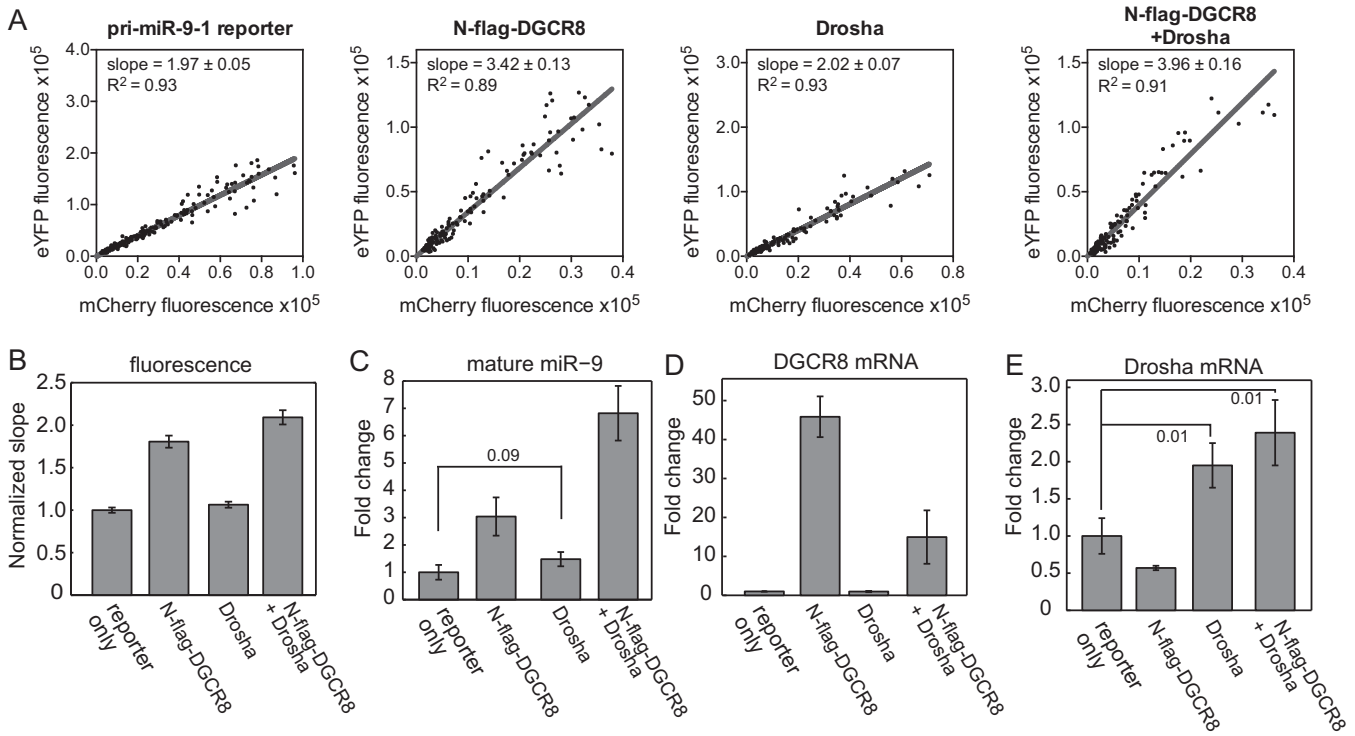

Fig. S4. Overexpression of Drosha does not enhance pri-miR9-1 processing. The pri-miR-9-1 reporter was transfected to HeLa cells either alone or with pN-flag-DGCR8, pCK-Drosha-Flag, or both. Cells were imaged, and RNA was extracted 18–20 h posttransfection. (*A*) Scatter plots showing the eYFP and mCherry fluorescence signals for individual cells and corresponding linear fits. The ratio of *y* and *x* axes was set at 4:1. (*B*) The normalized eYFP/mCherry fluorescence slope. The error bars represent 95% CI. (*C*) Mature miR-9 expression levels were measured using qRT-PCR. Error bars show SD ($n = 3$), except for N-flag-DGCR8, and "N-flag-DGCR8 + Drosha" ranges from two experiments are indicated. Total DGCR8 (*D*) and Drosha (*E*) expression levels, including expression from both endogenous genes and the plasmids, were measured using qRT-PCR. Shown are averages ± SD ($n = 3$). *P* values are labeled on the graphs.

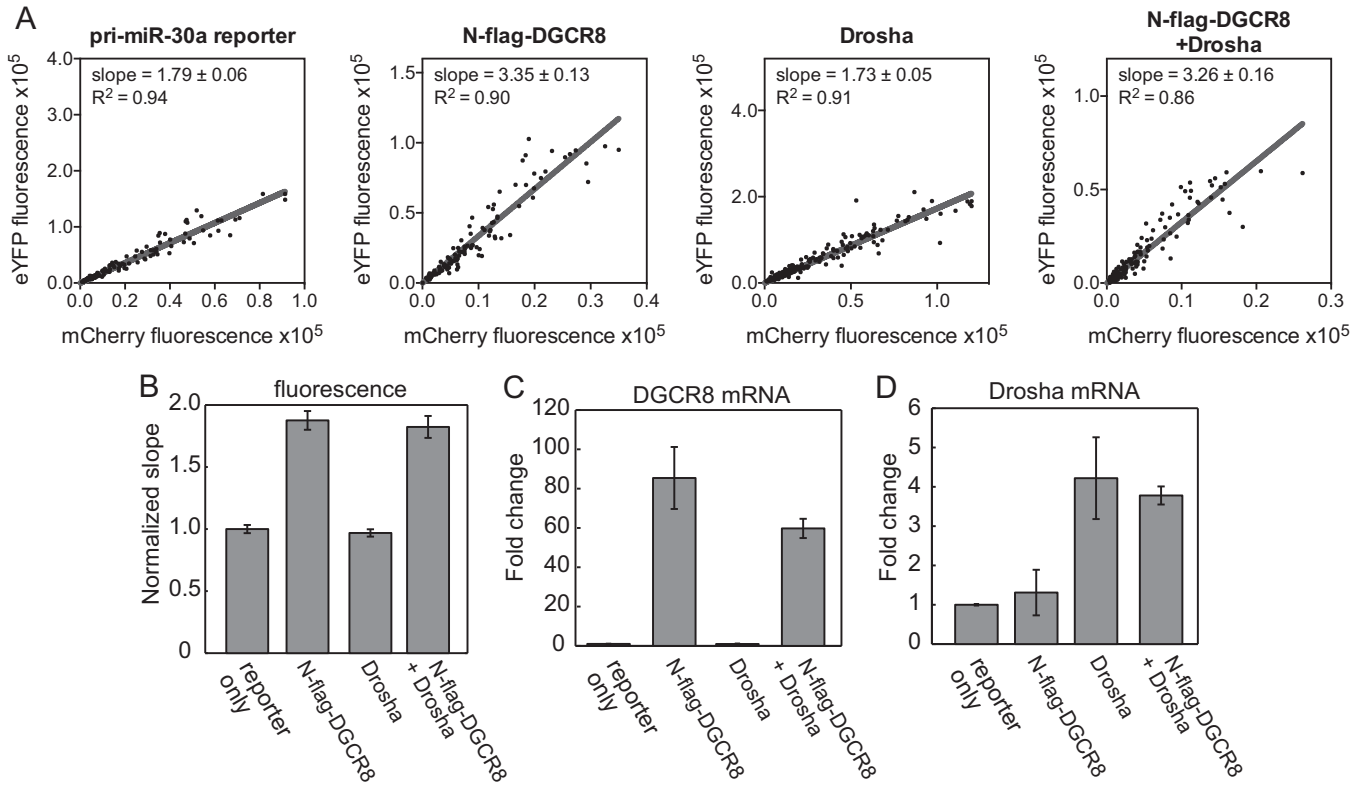

Fig. S5. Overexpression of Drosha does not enhance pri-miR-30a processing. The pri-miR-30a reporter was transfected to HeLa cells either alone or with pN-flag-DGCR8, pCK-Drosha-Flag, or both. (*A*) Scatter plots showing the eYFP and mCherry fluorescence signals for individual cells and corresponding linear fits. The ratio of *y* and *x* axes was set at 4:1. (*B–D*) The normalized eYFP/mCherry fluorescence slopes (*B*), DGCR8 (*C*), and Drosha (*D*) expression levels are plotted. Error bars in *A* represent 95% CI of the linear regression and in other panels show SD ($n = 3$).

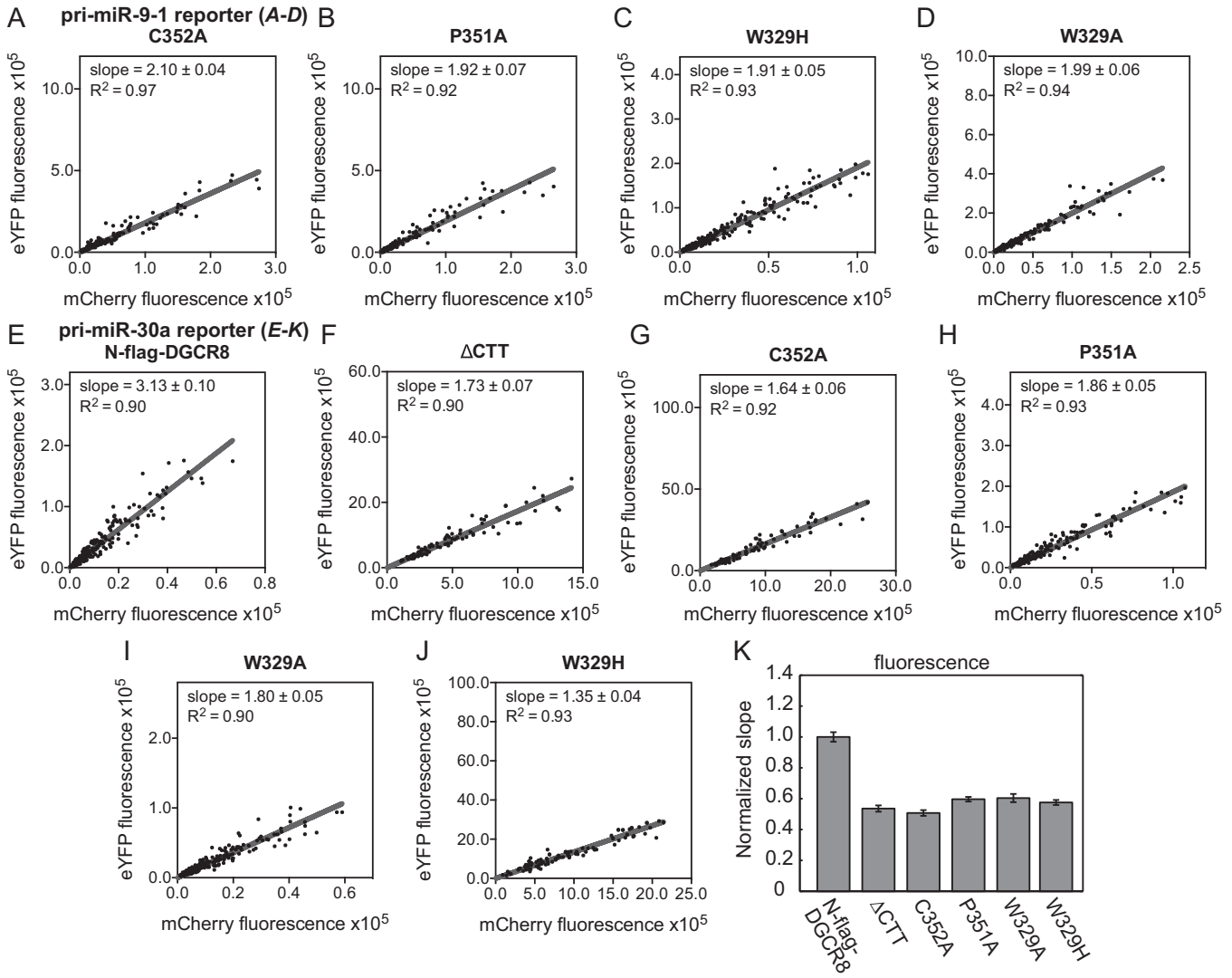

Fig. S6. All known heme-binding–deficient DGCR8 mutants are defective in cells. (*A–D*) Fluorescence scatter plots for the examination of heme-binding–deficient mutants as in Fig. 3 *A* and *F*. (*A*) C352A, (*B*) P351, (*C*) W329H, (*D*) W329A. The ratio of *y* and *x* axes was set at 4:1 for all scatter plots. Scatter plots for the corresponding N-flag-DGCR8 and ΔCTT transfections are shown in Fig. S1 *A* and *B*. (*E–K*) Examination of the DGCR8 mutants using the pri-miR-30a reporter confirms. Scatter plots of the eYFP and mCherry fluorescence signals for individual cells and corresponding linear fit for HeLa cells transfected with pri-miR-30a reporter and pN-flag-DGCR8 (*E*), ΔCTT (*F*), C352A (*G*), P351A (*H*), W329A (*I*), or W329H (*J*). (*K*) Shown are normalized eYFP/mCherry fluorescence slopes from transfections with the pri-miR-30a reporter and the indicated N-flag-DGCR8 expression plasmids. Error bars represent 95% CI from linear regression.

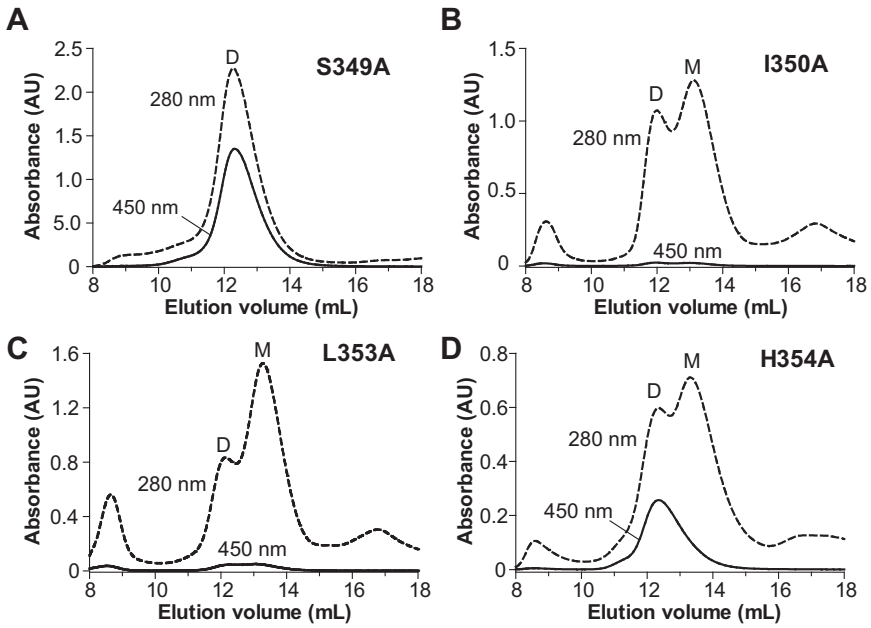

Fig. S7. Identification of a heme-binding motif in DGCR8. Mutant NC1 proteins were overexpressed in *E. coli* with 1 mM δ-ALA added at the time of induction. They were purified using a procedure described previously (5). The size exclusion chromatograms from the last step of the purification are shown. Before this step, the proteins were already over 90% pure. (*A*) S349A. (*B*) I350A. (*C*) L353A. (*D*) H354A. Dimer and "monomer" peaks are labeled as "D" and "M," respectively. The "monomer" species may not be biologically relevant, as it contains heterodimers in which one NC1 subunit is cleaved by bacterial proteases so that only the dimerization domain region remains, and the other NC1 subunit is intact.

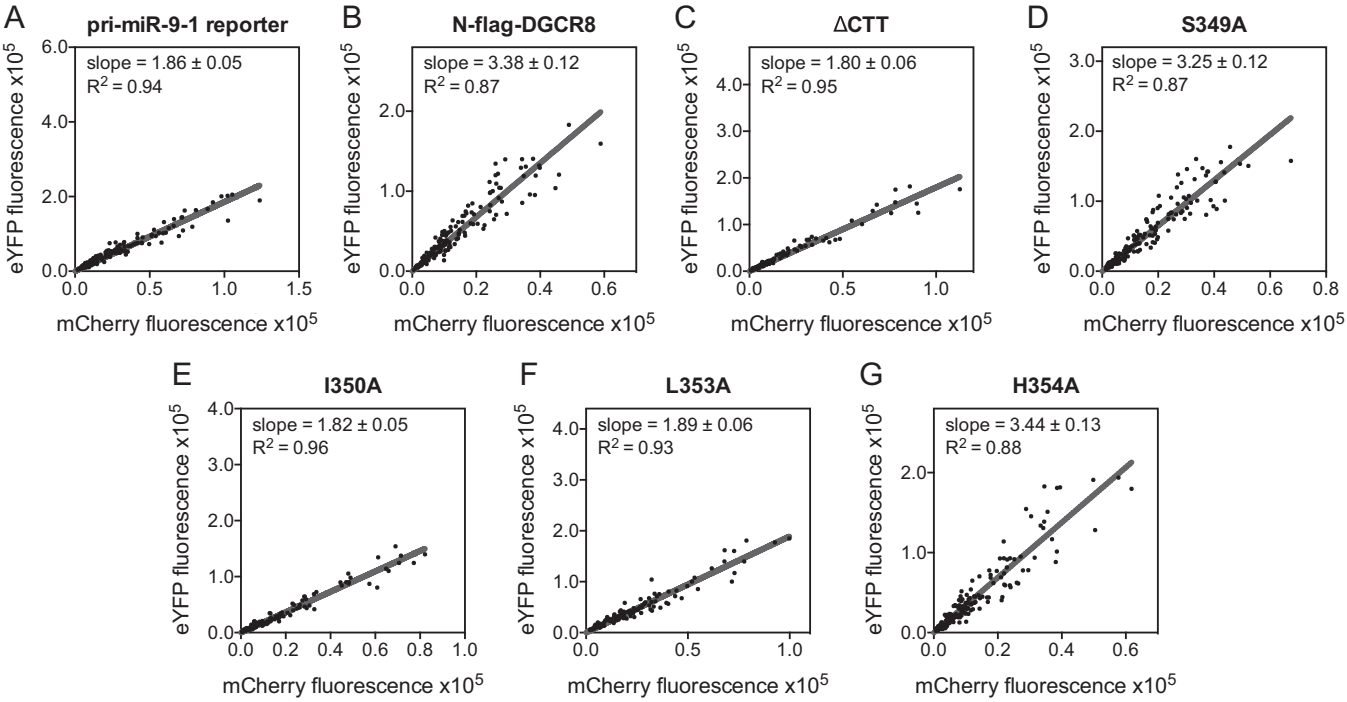

Fig. S8. Fluorescence scatter plots for the examination of DGCR8 mutations in or around the IPCL motif as in Fig. 4. The pri-miR-9-1 reporter was transfected to HeLa cells either alone (*A*) or with pN-flag-DGCR8 (*B*), ΔCTT (*C*), S349A (*D*), I350A (*E*), L353A (*F*), or H354A (*G*). The ratio of *y* and *x* axes was set at 4:1 for all plots.

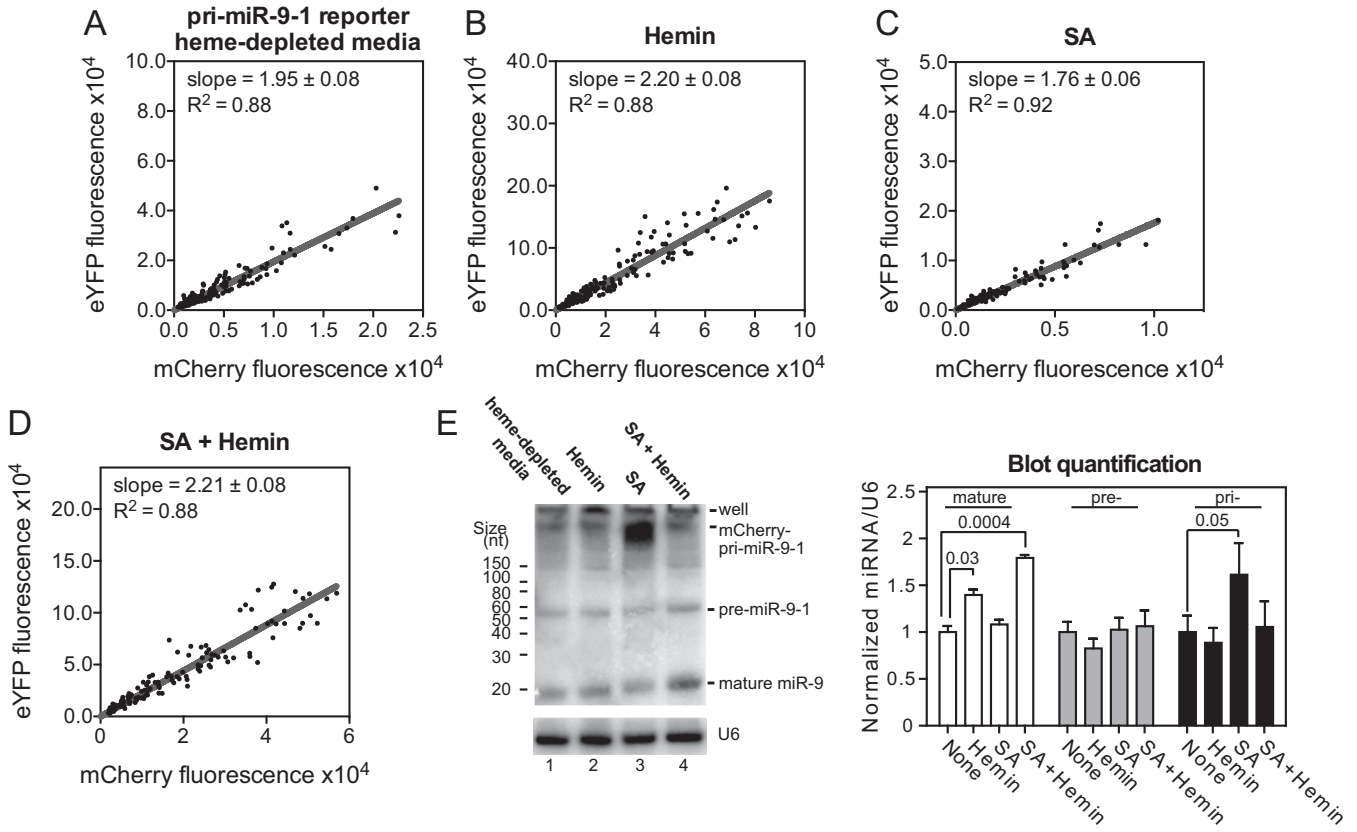

Fig. S9. Additional data to show that heme availability and biosynthesis in cells affect pri-miRNA processing. (*A*–*D*) Fluorescence scatter plots for Fig. 5*A*. HeLa cells were grown in heme-depleted media and transfected with the pri-miR-9-1 reporter, with no chemical treatment (*A*), or treated for 10 h with either hemin (*B*), or succinylacetone (*C*), or both (*D*). The ratio of *y* and *x* axes was set at 4:1 for all scatter plots. (*E*) Northern blot analyses of total RNAs. The pri-, pre-, and mature miR-9 levels, after normalization to those of U6 snRNA, are plotted on the *Right*.

Table S1. Identification of IPCL as a heme-binding motif

DGCR8 construct	Heme-bound	Heme removal by apomyoglobin	Reconstitution of heme complex
WT	Y	N	Y
S349A	Y	N	—
I350A	N	—	N
P351A	Y	Y	Y
C352A	N	—	N
L353A	N	—	N
H354A	Y	N	—

N, no; Y, yes; —, not tested.